

TABLE 1
 THE *VI* PHOTOMETRY AND RELATIVE PROPER MOTIONS OF THE MEMBER STARS ON THE PC CHIP OF
 WFPC2 (ONLINE TABLE 2).

No.	<i>X</i>	<i>Y</i>	<i>V</i>	<i>I</i>	<i>r</i> ($''$)	μ_x (mas/yr)	μ_y (mas/yr)
1	430.97	515.83	15.31	13.79	4.16	-0.32063	0.42928
2	707.94	502.85	15.24	13.60	13.74	-0.37145	-0.52531
3	79.76	548.09	15.25	13.70	16.59	-0.06742	0.05419
4	385.40	354.77	15.10	13.60	3.63	0.05419	0.22629
5	444.91	284.16	15.25	13.71	6.64	0.14993	-0.08465
6	279.54	568.62	15.45	13.93	9.17	-0.04913	0.32400
7	557.71	456.41	15.31	13.77	6.52	-0.06514	0.08690
8	407.94	298.04	15.43	13.88	5.92	0.18306	0.26771
9	516.83	420.49	15.60	14.01	4.50	-0.25409	0.29719
10	279.54	568.62	15.42	13.93	9.17	-0.04913	0.32400
11	456.94	492.47	15.49	14.01	3.51	0.12929	0.45399
12	544.61	364.36	15.47	13.95	6.43	0.21759	0.35839
13	635.45	511.55	15.71	14.15	10.70	-0.19092	0.01979
14	617.10	474.51	15.57	13.97	9.37	-0.01656	-0.18250
15	529.95	486.75	15.62	14.07	5.81	-0.03313	-0.06219
16	307.54	535.20	15.57	14.14	7.18	0.23008	0.34927
17	621.77	258.26	16.07	14.27	12.11	0.14319	0.10486
18	111.78	470.14	15.69	14.19	14.28	0.17895	0.37945
19	401.23	486.53	15.90	14.45	2.89	0.21113	0.12059
20	113.38	486.10	15.80	14.23	14.33	0.07268	0.13336
21	460.79	473.05	16.02	14.53	2.88	-0.31459	-0.09939
22	512.66	392.70	16.41	14.26	4.57	-0.03173	0.12227
23	327.54	484.04	16.08	14.58	4.98	-0.86166	0.29901
24	445.04	601.72	15.91	14.40	8.16	0.00969	0.46382
25	284.47	448.25	16.00	14.49	6.28	-0.31094	0.21296
26	273.67	439.32	16.21	14.42	6.72	-0.49077	0.22405
27	444.34	510.54	16.32	14.81	4.05	-0.63803	0.38001
28	78.40	300.69	16.16	14.53	16.70	-0.02625	0.09012
29	391.77	478.92	16.16	14.68	2.73	0.16284	0.18951
30	350.35	341.22	16.07	14.52	5.03	0.04183	0.12831
31	243.53	570.81	16.15	14.65	10.46	-0.03720	0.16790
32	206.53	509.92	16.12	14.64	10.51	-0.29852	0.14431
33	464.23	466.28	16.23	14.73	2.77	-0.22952	0.42044
34	464.23	238.36	16.34	14.76	8.89	0.17337	0.26125
35	286.48	587.12	16.57	14.70	9.59	-0.10023	0.65642
36	504.90	503.73	16.24	14.71	5.32	-0.16242	-0.06429
37	489.07	675.78	16.46	14.68	11.92	0.34127	0.29508
38	230.44	136.61	16.60	14.86	15.90	0.55240	0.11455
39	572.25	340.07	16.47	14.78	8.08	-0.14235	0.53303
40	522.21	564.68	16.46	14.83	7.94	0.23612	0.08142
41	210.33	156.48	16.70	14.97	15.69	0.51471	0.24840

TABLE 1—*Continued*

No.	X	Y	V	I	r (")	μ_x (mas/yr)	μ_y (mas/yr)
42	317.97	375.49	16.66	14.77	5.21	-0.11638	0.59072
43	502.33	376.68	16.56	14.98	4.45	0.15512	0.13856
44	766.53	443.54	16.67	15.03	16.00	-0.15695	-0.36850
45	401.53	512.21	17.44	15.32	4.04	-0.69910	0.00449
46	451.09	399.54	17.06	15.25	1.91	-0.17351	-0.77827
47	505.32	258.49	16.77	15.14	8.67	-0.03580	0.17239
48	376.85	433.00	16.64	15.13	1.97	-0.19738	0.21984
49	339.71	440.82	16.63	15.10	3.72	-0.28750	0.11273
50	213.40	397.73	16.88	14.83	9.55	-0.29122	0.39138
51	250.75	313.46	16.59	14.94	9.32	0.06071	0.35881
52	508.77	415.49	17.03	15.40	4.15	-0.29522	0.06429
53	553.60	460.42	16.83	15.19	6.38	-0.00590	0.27332
54	476.66	441.44	17.09	15.50	2.74	-0.01474	0.68716
55	458.81	631.43	16.98	14.97	9.61	0.32807	0.41946
56	182.45	455.58	16.64	15.07	10.97	-0.31193	-0.01741
57	574.46	582.99	16.84	15.18	10.15	-0.37426	0.04296
58	381.50	256.05	16.89	15.22	8.02	-0.35278	0.11638
59	359.85	620.92	17.49	15.35	9.36	0.45217	0.30771
60	282.83	503.05	16.65	15.18	7.20	-0.43476	-0.05377
61	390.49	543.12	17.46	15.56	5.54	-0.19962	-0.47954
62	379.32	246.33	16.95	15.19	8.48	-0.00365	0.18355
63	486.73	425.43	16.85	15.24	3.11	-0.02808	0.38450
64	484.66	300.92	16.94	15.29	6.50	-0.21254	0.28203
65	435.64	515.56	17.09	15.55	4.18	0.10908	0.26897
66	558.53	473.92	17.09	15.49	6.78	0.10585	0.25030
67	244.54	139.89	17.17	15.48	15.43	0.32842	0.10809
68	146.55	393.10	16.92	15.29	12.63	-0.06345	0.14768
69	540.35	668.07	17.15	15.28	12.44	-0.43799	0.19681
70	411.99	403.55	17.19	15.62	1.09	0.18250	0.24651
71	519.81	297.07	17.20	15.35	7.53	-0.07833	0.67607
72	320.04	447.85	17.05	15.51	4.67	-0.12971	0.48403
73	299.46	703.65	17.26	15.60	13.90	0.86208	0.70668
74	250.97	496.05	16.99	15.45	8.38	-0.08605	-0.29115
75	150.01	446.89	17.11	15.59	12.42	-0.32982	-0.09012
76	356.35	271.34	17.13	15.53	7.69	0.04562	0.38310
77	572.93	791.49	17.39	15.63	18.23	-0.84397	0.79428
78	270.57	441.35	17.54	15.95	6.87	-0.44950	0.48445
79	473.68	382.05	17.30	15.69	3.23	0.10809	0.17056
80	752.85	244.18	17.19	15.56	17.49	0.75441	0.37854
81	314.85	525.04	17.31	15.66	6.61	-0.27781	0.16228
82	604.62	451.54	17.30	15.70	8.61	0.45427	-0.31277

TABLE 1—*Continued*

No.	X	Y	V	I	r''	$\mu_x(\text{mas/yr})$	$\mu_y(\text{mas/yr})$
83	568.64	233.36	17.62	15.64	11.22	-0.22854	-0.11273
84	521.79	476.31	17.52	15.74	5.25	-0.35292	-0.29213
85	555.38	670.06	17.41	15.60	12.85	-0.53317	-0.09518
86	151.26	451.30	17.66	15.76	12.38	0.07173	0.03130
87	451.83	568.40	17.26	15.70	6.71	-0.27374	-0.28890
88	511.70	159.67	17.68	15.83	12.98	0.21998	-0.22033
89	604.04	218.05	17.48	15.84	12.81	0.00646	0.44711
90	449.27	215.57	17.39	15.71	9.79	0.19780	0.24609
91	670.74	386.80	17.48	15.85	11.71	-0.09939	0.01334
92	193.08	584.60	17.37	15.87	12.70	0.01699	0.09153
93	671.99	184.11	17.67	15.76	16.10	0.32175	0.03629
94	467.53	605.53	17.62	15.99	8.54	0.41497	0.25325
95	557.67	470.34	17.81	16.13	6.69	0.36920	0.30266
96	543.90	442.44	17.80	16.11	5.79	-0.08928	-0.23135
97	517.16	241.73	17.58	15.97	9.61	-0.02555	0.13343
98	193.34	554.39	17.62	16.04	11.94	-0.12375	-0.54552
99	409.75	345.83	17.78	16.12	3.72	0.07581	0.22812
100	477.45	543.01	17.56	15.97	6.00	0.25170	-0.33130
101	316.49	413.99	17.57	15.97	4.76	-0.21998	-0.01334
102	357.70	534.96	17.75	16.21	5.75	-0.47322	-0.23191
103	391.92	654.89	17.96	16.13	10.59	0.33621	-0.03173
104	510.25	472.14	17.84	16.20	4.69	0.01656	0.38226
105	461.91	527.86	17.73	16.17	5.07	0.01979	0.18502
106	250.08	586.77	17.70	16.06	10.73	0.12003	0.18699
107	497.25	528.50	17.81	16.16	5.92	-0.16888	0.01067
108	564.22	162.64	17.69	16.12	13.84	0.08282	-0.29529
109	427.06	127.39	17.82	16.20	13.75	0.10023	-0.59936
110	264.47	598.97	17.84	16.29	10.67	0.18811	0.01544
111	353.77	218.74	17.97	16.32	10.01	0.13799	0.15547
112	495.22	666.32	18.05	15.64	11.59	0.03229	0.25942
113	455.06	364.98	17.93	16.29	3.27	-0.66976	-0.22124
114	470.14	230.05	18.01	15.91	9.32	0.13252	-0.15547
115	179.39	681.67	18.14	16.21	16.12	0.48488	0.49583
116	575.56	539.14	18.07	16.08	8.87	-0.08367	-0.22826
117	571.41	188.10	18.22	16.21	13.00	-0.20468	-0.19962
118	198.09	379.40	17.99	16.11	10.39	-0.01607	0.22910
119	603.89	188.19	18.02	16.34	13.86	-0.08142	-0.09019
120	312.83	676.51	18.15	16.40	12.51	0.30168	0.03594
121	386.64	426.83	18.07	16.18	1.50	0.39096	0.40023
122	655.30	382.07	18.16	16.45	11.05	-0.02583	0.02667
123	562.86	303.39	18.24	16.58	8.70	-0.33635	0.04913

TABLE 1—*Continued*

No.	X	Y	V	I	r (")	μ_x (mas/yr)	μ_y (mas/yr)
124	331.55	619.25	18.06	16.44	9.75	0.16551	0.28188
125	684.28	368.62	18.18	16.47	12.48	0.35376	0.06219
126	611.78	306.67	18.15	16.42	10.43	0.10725	0.37636
127	622.19	143.00	18.06	16.46	16.03	0.11455	-0.42732
128	653.65	341.11	18.21	16.51	11.48	0.15582	0.35923
129	435.61	237.91	18.00	16.35	8.70	-0.14726	0.08191
130	666.45	601.80	18.19	16.39	13.95	-0.97424	-0.14740
131	373.24	178.94	18.15	16.31	11.57	0.41075	0.00232
132	502.23	531.60	18.32	16.63	6.17	-0.17885	0.14291
133	101.71	572.66	18.18	16.53	16.08	0.27371	-0.37341
134	234.41	525.98	18.08	16.47	9.66	-0.22959	-0.24679
135	527.26	464.69	18.36	16.65	5.28	0.03622	0.08226
136	213.02	369.59	18.05	16.46	9.83	-0.15828	0.03495
137	250.01	539.40	18.13	16.54	9.36	-0.45722	-0.43293
138	618.62	555.78	18.20	16.52	10.94	-0.07833	-0.19288
139	599.73	231.76	18.75	16.44	12.21	0.34534	-0.10718
140	479.53	379.96	18.20	16.55	3.50	-0.03636	-0.13112
141	397.68	634.78	18.98	16.51	9.64	0.24791	-0.12747
142	760.66	435.76	18.44	16.71	15.72	-0.45511	-0.64631
143	245.66	347.20	18.19	16.57	8.77	-0.21254	0.42830
144	143.99	486.59	18.28	16.66	12.96	-0.39742	-0.34786
145	497.53	735.73	18.56	16.57	14.69	0.20060	0.72802
146	409.92	315.33	19.26	16.75	5.12	0.16649	0.14908
147	343.81	790.84	18.59	16.83	17.13	0.92693	0.93157
148	242.07	484.76	18.77	16.64	8.58	-0.19366	-0.10121
149	731.05	433.17	18.52	16.80	14.35	-0.08844	-0.01713
150	473.15	474.39	18.30	16.62	3.33	-0.36948	0.17520
151	222.98	408.93	18.27	16.68	9.06	-0.08739	0.13982
152	145.19	501.83	18.37	16.69	13.07	0.04099	-0.16242
153	351.87	471.22	18.30	16.37	3.72	-0.01095	0.09335
154	300.08	353.20	18.37	16.72	6.43	-0.37032	0.22264
155	573.05	265.03	19.03	17.04	10.25	0.14656	-0.20524
156	441.97	649.70	18.89	16.80	10.33	0.34913	0.35292
157	419.03	397.64	18.67	17.04	1.31	-0.34913	-0.08423
158	382.21	423.33	18.38	16.73	1.70	-0.40009	0.19597
159	491.39	518.76	18.57	16.94	5.40	0.01558	0.03594
160	280.30	594.79	18.47	16.92	10.05	0.09981	0.35488
161	403.15	195.38	18.59	16.89	10.64	0.03032	0.14122
162	52.95	493.82	19.27	16.87	17.13	0.18579	-0.79161
163	554.81	427.33	19.39	16.89	6.24	0.42479	-0.09518
164	710.68	449.69	18.73	17.00	13.45	-0.53597	-0.25255

TABLE 1—*Continued*

No.	X	Y	V	I	r''	$\mu_x(\text{mas/yr})$	$\mu_y(\text{mas/yr})$
165	229.32	382.84	18.83	16.86	8.96	-0.30638	0.47056
166	522.65	396.29	19.80	17.11	4.96	-0.09012	-0.24426
167	294.38	237.72	19.00	16.83	10.40	0.18081	0.21022
168	381.34	322.34	18.78	17.09	5.09	-0.05334	0.19232
169	616.79	586.90	19.84	16.99	11.72	-0.30294	-0.43546
170	240.35	400.95	19.67	16.96	8.31	-0.58511	-0.22910
171	270.03	453.71	19.98	17.29	6.98	-0.84860	-0.11722
172	405.76	104.51	18.79	17.10	14.81	0.32849	-0.75118
173	608.04	127.54	18.91	17.16	16.26	0.10388	-0.65688
174	291.79	637.15	19.66	16.94	11.33	0.32568	-0.01656
175	574.51	366.38	19.78	17.05	7.66	0.17716	0.08240
176	290.31	282.35	18.82	17.08	8.88	0.39152	0.10543
177	377.34	446.03	18.43	16.77	2.13	0.01755	0.42648
178	131.16	629.49	19.85	17.24	16.22	0.09335	0.13280
179	362.71	704.77	19.06	17.33	13.07	0.52811	0.56854
180	234.71	412.42	19.62	17.14	8.51	-0.39335	0.12592
181	381.51	415.86	18.60	16.92	1.80	-0.24328	0.30449
182	546.06	189.09	19.05	17.33	12.37	0.36948	-0.29992
183	726.07	416.65	19.32	17.53	14.13	0.06317	-0.41623
184	401.07	301.89	20.17	17.48	5.78	-0.51843	0.17941
185	383.01	623.72	19.68	17.29	9.24	0.25662	0.28160
186	551.70	411.56	20.06	17.39	6.13	0.13336	0.07763
187	577.22	744.61	19.67	17.45	16.35	-0.75497	-0.13027
188	638.51	183.63	19.23	17.49	15.04	0.02583	-0.05608
189	540.50	694.19	19.90	17.56	13.53	0.27655	0.25240
190	335.88	578.06	20.14	17.44	7.97	-0.06219	-0.21029
191	143.77	267.34	19.93	17.40	14.62	-0.03727	0.36008
192	168.84	314.35	19.27	17.47	12.61	0.23921	0.09532
193	283.33	574.14	19.71	17.71	9.24	0.71749	0.33860
194	326.00	287.11	20.18	17.49	7.70	-0.10529	0.36892
195	100.00	403.04	19.35	17.47	14.72	0.28750	-0.17014
196	731.38	269.55	20.12	17.45	16.07	0.53962	0.16017
197	680.15	535.04	20.45	17.66	13.01	-0.25549	-0.61318
198	119.14	437.01	19.94	17.43	13.81	-0.07268	-0.36653
199	497.98	232.01	19.42	17.68	9.64	0.15638	-0.26686
200	504.09	629.38	19.49	17.57	10.13	0.10851	-0.04885
201	506.81	430.19	20.45	17.68	4.04	-0.77925	0.51071
202	378.11	171.24	19.38	17.68	11.88	0.13673	-0.07082
203	256.40	594.80	20.37	17.68	10.78	0.21198	0.08591
204	234.24	377.92	20.26	17.63	8.79	-0.24054	-0.15596
205	101.74	352.14	19.58	17.70	14.99	-0.10858	0.11090

TABLE 1—*Continued*

No.	X	Y	V	I	r ($''$)	μ_x (mas/yr)	μ_y (mas/yr)
206	566.42	620.90	20.60	17.81	11.23	-0.23724	-0.13926
207	689.64	369.47	19.47	17.91	12.71	0.32288	-0.44304
208	490.24	376.90	20.36	17.70	3.98	-0.00730	0.15919
209	340.77	530.73	20.58	18.03	6.01	-0.50930	0.14431
210	546.62	496.01	19.60	17.82	6.68	-0.23640	-0.20468
211	117.87	638.09	20.97	18.03	16.94	0.11778	-0.66035
212	563.43	724.04	20.49	17.83	15.22	-0.68955	0.03706
213	159.79	308.04	20.61	17.88	13.11	0.19415	0.11188
214	157.63	628.02	20.43	17.83	15.19	0.33993	-0.58511
215	512.09	179.66	19.89	18.07	12.12	0.49175	-0.95354
216	459.75	766.73	19.85	18.03	15.77	0.55156	0.57472
217	675.83	519.51	20.96	18.14	12.56	-0.73082	-0.44248
218	258.53	486.98	20.65	17.86	7.90	-0.07637	-0.22124
219	313.93	596.28	20.39	17.92	9.20	0.22489	-0.15835
220	425.45	560.04	20.47	17.75	6.16	-0.15877	-0.07946
221	204.88	370.95	20.66	17.91	10.18	-0.09981	-0.01011
222	453.90	502.19	20.86	17.92	3.84	-0.19134	-0.33902
223	382.37	528.90	19.50	17.24	5.02	-0.00646	-0.55029
224	242.65	433.90	20.59	17.90	8.13	-0.61683	-0.20145
225	402.07	287.19	20.95	18.19	6.44	0.12873	-0.20608
226	331.25	515.62	20.55	17.89	5.77	-0.07216	0.04520
227	547.83	500.57	20.87	18.09	6.84	0.03257	-0.12564
228	307.16	734.36	21.42	18.30	15.08	1.08192	0.43518
229	363.68	184.93	21.15	18.21	11.39	-0.07047	-0.07082
230	236.32	486.55	21.03	18.19	8.86	-0.22215	-0.11680
231	422.46	586.79	20.79	18.04	7.39	-0.05292	0.44248
232	350.02	555.14	20.81	18.19	6.73	-0.40107	-0.17211
233	95.01	358.38	20.90	18.07	15.23	-0.07816	0.07272
234	428.68	561.42	20.32	17.67	6.23	-0.02850	-0.07946
235	641.32	161.10	20.95	18.27	15.91	0.16677	-0.45266
236	540.91	607.99	20.31	18.47	10.06	0.23893	-0.03229
237	466.77	272.93	21.14	18.33	7.38	0.32105	0.10346
238	688.51	254.40	21.06	18.30	14.70	0.20917	-0.38177
239	706.83	337.01	21.36	18.54	13.85	0.16144	-0.21899
240	250.16	131.29	21.47	18.47	15.64	0.28883	-0.28434
241	423.77	182.03	20.30	18.42	11.23	-0.02625	-0.07314
242	240.92	418.74	20.74	18.43	8.21	0.64259	-0.58005
243	127.84	489.44	20.63	18.49	13.71	-0.27785	-0.10753
244	562.75	136.24	20.56	18.54	14.89	0.62469	-0.75665
245	431.40	730.28	20.54	18.71	14.00	0.46649	0.57472
246	219.06	233.82	21.41	18.53	12.77	0.24658	0.18860

TABLE 1—*Continued*

No.	X	Y	V	I	r (")	μ_x (mas/yr)	μ_y (mas/yr)
247	426.46	587.68	20.64	18.05	7.43	-0.41581	-0.11427
248	592.99	549.44	21.65	18.67	9.80	-0.16565	-0.11680
249	407.14	554.03	20.67	17.86	5.91	0.32428	-0.15358
250	404.25	677.95	21.31	18.69	11.60	0.29480	0.22517
251	225.81	373.98	21.63	18.80	9.21	-0.15821	-0.31866
252	238.35	435.13	21.67	18.72	8.33	-0.66702	0.14894
253	403.79	155.25	20.59	18.67	12.48	-0.46143	-0.66976
254	484.29	248.52	21.48	18.79	8.71	0.14572	0.14993
255	90.01	592.62	21.71	18.82	16.97	-0.41153	-0.39559
256	599.69	302.53	21.88	18.83	10.07	0.27908	-0.10248
257	186.43	496.98	22.11	18.99	11.19	-0.26960	-0.48614
258	327.61	278.30	21.71	18.71	8.00	-0.14038	0.36667
259	197.21	450.92	22.06	19.01	10.27	-0.17569	-0.04787
260	131.38	452.85	21.73	18.77	13.29	-0.03587	-0.19148
261	183.51	507.34	21.60	18.79	11.46	-0.30680	-0.71019
262	649.41	211.26	21.70	18.91	14.49	0.48319	-0.11406
263	486.86	418.10	21.52	18.46	3.14	-0.21857	-0.46747
264	309.93	136.43	21.82	18.95	14.25	0.03173	-0.29901
265	531.46	724.53	21.10	19.07	14.66	0.22321	0.47786
266	465.79	723.09	22.35	19.16	13.82	0.06710	-0.12269
267	470.67	620.37	21.77	18.98	9.24	0.12143	-0.13870
268	232.22	419.38	21.86	18.90	8.60	-0.56672	0.25255
269	87.98	542.33	21.84	18.70	16.14	0.47930	-0.31417
270	574.17	601.13	22.32	19.14	10.75	-0.25325	0.07974
271	559.22	530.71	21.81	19.02	8.04	0.03762	-0.07665
272	110.24	389.10	22.32	19.25	14.31	0.16425	-0.07272
273	706.85	345.66	21.59	19.04	13.74	-0.12606	0.46227
274	350.83	563.06	21.71	18.84	7.04	0.03720	-0.29424
275	371.11	309.50	21.86	18.89	5.81	-0.03215	0.37201
276	252.77	545.45	21.91	18.97	9.42	0.22587	-0.30322
277	294.07	344.15	21.96	19.04	6.88	-0.22447	0.20060
278	492.61	136.02	22.29	19.21	13.77	0.22629	-0.86573
279	504.27	244.87	22.08	19.08	9.22	0.03720	0.54145
280	598.15	470.15	22.08	19.07	8.48	-0.33579	-0.49175
281	535.65	471.43	21.73	18.96	5.75	-0.35601	-0.27318
282	203.54	291.56	21.86	19.15	11.69	0.01614	0.45175
283	130.39	548.45	22.21	19.33	14.42	0.07223	-0.59802
284	565.69	475.11	21.91	18.97	7.11	0.16425	0.11357
285	374.71	193.74	21.93	19.27	10.89	0.28385	0.30870
286	172.11	551.78	22.07	19.19	12.75	-0.33347	-0.74851
287	382.03	311.09	22.31	19.22	5.56	0.58286	0.16060

TABLE 1—*Continued*

No.	X	Y	V	I	r (")	μ_x (mas/yr)	μ_y (mas/yr)
288	518.54	375.99	22.20	19.22	5.12	0.27374	0.21984
289	542.15	430.54	21.91	18.95	5.66	-0.17491	-0.08647
290	390.34	314.54	22.08	19.02	5.31	0.04141	0.08605
291	312.83	713.58	22.26	19.44	14.09	0.43925	-0.31698
292	162.72	606.54	22.05	19.35	14.42	0.04548	-0.99642
293	185.59	676.73	21.53	19.02	15.76	0.30771	0.19541
294	350.87	227.09	22.67	19.36	9.68	-0.21212	0.06212
295	575.71	373.76	22.37	19.33	7.60	0.22742	0.29073
296	395.04	133.17	22.46	19.33	13.53	-0.25212	-0.68730
297	331.37	730.53	22.62	19.49	14.57	0.95585	-0.44220
298	377.08	600.84	22.22	19.25	8.26	0.13168	0.12325
299	377.58	676.63	22.36	19.44	11.68	0.62090	-0.24482
300	584.51	403.87	22.44	19.40	7.68	-0.15807	-0.19639
301	369.68	336.49	22.29	19.37	4.71	-0.21113	0.32007
302	85.75	450.33	22.77	19.60	15.38	-0.40416	-0.46452
303	573.63	350.44	22.03	19.33	7.91	-0.02021	0.46410
304	230.44	615.37	22.16	19.41	12.29	0.08788	-0.67523
305	157.54	461.24	22.30	19.32	12.14	-0.39559	-0.17393
306	105.12	621.86	22.20	19.45	17.02	0.04829	-0.93437
307	385.25	392.83	21.92	19.03	2.19	-0.31796	-0.39559
308	463.12	589.64	21.95	19.12	7.78	0.30084	0.30042
309	255.82	417.31	22.68	19.57	7.52	-0.21113	0.03734
310	269.30	658.02	21.82	19.59	12.70	0.44978	0.07187
311	451.33	725.92	21.57	19.71	13.87	0.19499	-0.84341
312	468.90	348.70	22.27	19.38	4.24	-0.38549	-0.24103
313	352.97	565.98	22.49	19.49	7.11	-0.51927	-0.06851
314	479.29	553.63	22.08	19.43	6.48	-0.98309	-0.22573
315	225.82	307.63	22.50	19.59	10.43	0.46922	0.32105
316	417.98	133.75	22.93	19.73	13.45	0.56588	-0.68906
317	491.65	221.39	23.02	19.71	9.99	-0.10500	-0.37257
318	500.55	509.52	22.32	19.21	5.36	-0.17660	-0.73040
319	310.01	634.66	22.49	19.46	10.82	0.61585	0.10472
320	493.72	141.20	22.36	19.32	13.55	0.02766	-0.74472
321	328.22	643.91	22.77	19.86	10.85	0.61234	-0.63284
322	182.95	444.14	23.13	19.84	10.90	-0.51562	-0.01151
323	63.96	479.98	22.77	19.71	16.52	0.29159	-0.42872
324	269.99	380.50	22.57	19.64	7.18	0.08647	0.39966
325	286.80	493.20	22.65	19.66	6.82	-0.16649	-0.74921
326	340.32	185.16	22.72	19.84	11.67	0.06078	0.37994
327	571.79	391.68	22.30	19.57	7.20	-0.49863	-0.57303
328	306.83	264.24	22.63	19.64	9.07	-0.15681	0.17295

TABLE 1—*Continued*

No.	X	Y	V	I	r''	$\mu_x(\text{mas/yr})$	$\mu_y(\text{mas/yr})$
329	458.58	345.75	22.36	19.63	4.12	0.16649	-0.04927
330	248.72	282.59	22.52	19.66	10.25	-0.02709	0.68211
331	216.86	587.50	22.50	19.70	11.90	0.16972	-0.69573
332	276.80	661.89	22.85	19.90	12.66	0.34492	0.28104
333	493.62	148.09	22.66	19.71	13.24	-0.03538	-0.69832
334	351.32	372.16	22.78	19.94	3.99	0.45638	-0.25942
335	314.21	634.73	22.86	19.78	10.74	0.12382	-0.58174
336	630.95	358.39	22.78	19.85	10.23	0.01320	-0.24609
337	518.27	514.03	22.64	19.80	6.09	0.76283	-0.59185
338	479.36	536.28	22.80	19.66	5.77	0.05012	-0.43883
339	197.39	541.10	22.90	19.89	11.49	0.30814	-1.04050
340	312.93	160.34	22.96	19.98	13.17	0.50832	-0.33488
341	630.16	230.87	22.80	19.83	13.23	-0.85183	0.18629
342	359.10	645.25	23.02	19.90	10.45	0.37075	0.24735
343	430.92	257.46	22.71	19.83	7.78	0.01011	0.07777
344	227.27	503.89	22.95	19.97	9.52	-0.08781	0.13617
345	494.82	542.73	23.13	19.93	6.39	0.08016	-0.29115
346	686.48	466.80	23.18	20.11	12.44	-0.29396	-0.46915
347	494.75	616.96	23.02	20.04	9.44	-0.09799	-0.83162
348	486.31	253.52	23.26	20.05	8.52	-0.41216	0.13013
349	513.33	224.84	23.14	20.13	10.23	-0.24482	-0.35558
350	251.46	220.78	22.87	19.87	12.20	0.19646	0.01930
351	491.54	196.42	22.88	19.76	11.08	0.23233	0.42409
352	526.76	442.33	23.00	20.12	5.01	0.72380	-0.85745
353	184.48	235.34	23.22	20.33	13.91	-0.03495	0.19366
354	670.90	196.29	22.87	20.17	15.68	0.65417	0.04001
355	479.29	101.17	23.28	20.06	15.21	-0.04955	-0.66976
356	593.33	539.75	23.19	20.16	9.56	0.87935	-0.29677
357	135.32	454.56	22.91	19.94	13.12	-0.92188	0.71580
358	385.40	354.77	15.10	13.60	3.63	0.05419	0.22629
359	440.93	405.71	11.92	10.32	1.38	-0.13799	0.04590
360	433.96	452.25	12.82	11.15	1.38	0.00000	0.32203
361	335.29	483.77	12.86	11.34	4.68	-0.50593	0.00000
362	406.67	507.55	13.09	11.56	3.78	0.00000	-0.18404
363	423.50	492.46	13.12	11.61	3.05	0.09195	0.55198
364	358.09	414.45	13.15	11.59	2.86	-0.23008	0.69011
365	411.37	509.35	13.32	11.80	3.84	0.00000	0.32203
366	306.55	575.18	13.18	11.70	8.59	0.22994	0.00000
367	430.67	443.18	13.22	11.66	0.94	0.13799	0.22994
368	360.83	482.14	13.33	11.85	3.72	-0.13799	-0.04590
369	424.64	481.43	13.46	11.90	2.55	0.09209	0.59802

TABLE 1—*Continued*

No.	X	Y	V	I	r ($''$)	μ_x (mas/yr)	μ_y (mas/yr)
370	592.23	510.22	13.57	11.96	8.85	0.18390	-0.18404
371	508.60	581.52	13.62	12.02	8.24	0.78206	0.04604
372	397.40	442.74	13.58	12.08	1.26	-0.13799	-0.23008
373	456.37	371.75	13.66	12.08	3.03	-0.13799	0.04604
374	451.85	453.88	13.70	12.12	1.97	0.04604	0.23008
375	328.58	495.70	13.93	12.46	5.25	-0.32203	-0.27599
376	415.71	490.41	14.31	12.81	2.96	-0.27599	-0.04604
377	519.94	282.52	13.81	12.26	8.07	0.00000	0.32189
378	400.62	351.65	14.04	12.49	3.53	-0.55198	-0.18404
379	458.24	569.57	13.97	12.46	6.83	0.27599	-0.22994
380	406.78	569.06	14.13	12.55	6.60	-0.04604	-0.45989
381	395.27	497.29	14.22	12.74	3.45	0.00000	-0.22994
382	391.78	549.92	14.20	12.71	5.83	0.36794	-0.09209
383	512.30	419.52	14.40	12.81	4.30	-0.09209	0.22994
384	296.12	315.53	14.26	12.65	7.61	-0.13799	0.87401
385	402.49	382.63	14.18	12.66	2.15	0.32189	-0.09195
386	397.69	446.10	14.35	12.76	1.35	-0.13799	0.18404
387	264.53	464.97	14.23	12.73	7.33	-0.82797	-0.41398
388	383.91	479.85	14.24	12.78	2.95	0.00000	0.09209
389	342.85	107.87	14.29	12.73	15.06	0.32203	0.13803
390	411.70	515.19	14.52	13.00	4.11	0.41412	0.50593
391	752.70	234.66	14.32	12.80	17.69	-0.13785	-0.09195
392	477.39	496.02	14.47	12.94	4.18	0.13813	-0.78206
393	336.64	433.13	14.96	13.46	3.81	-0.09195	0.00000
394	317.77	326.86	14.63	13.13	6.53	0.00000	-0.04604
395	343.07	484.10	14.85	13.34	4.40	-0.18390	-0.09195
396	676.63	327.21	15.07	13.56	12.69	0.27599	0.22994
397	302.45	467.14	14.61	13.07	5.69	-0.09195	-0.41398
398	652.42	324.93	14.93	13.42	11.70	0.04604	-0.32203
399	318.17	548.02	14.77	13.18	7.28	0.27613	-0.59802
400	391.70	470.68	14.76	13.19	2.40	-0.41398	-0.27599
401	547.33	266.18	14.74	13.21	9.43	-0.36780	-0.32203
402	385.12	538.86	14.88	13.35	5.41	0.59802	-0.55198
403	93.93	382.69	14.83	13.19	15.09	0.00000	-0.09195
404	385.31	354.76	15.22	13.71	3.64	0.09195	0.13799
405	631.82	261.16	14.84	13.35	12.38	-0.04604	-0.32203
406	473.73	446.04	14.95	13.35	2.67	-0.18390	-0.04590
407	525.52	360.33	14.89	13.35	5.76	0.18418	-0.09209
408	415.36	515.59	15.05	13.57	4.11	0.13799	0.32203
409	339.21	346.45	14.95	13.38	5.19	0.09195	-0.04590
410	451.68	490.01	14.96	13.44	3.29	-0.36808	-0.04590

□

TABLE 1—*Continued*

No.	X	Y	V	I	$r(\prime\prime)$	$\mu_x(\text{mas/yr})$	$\mu_y(\text{mas/yr})$
411	396.13	537.73	15.10	13.60	5.24	-0.04604	-0.27599

X and Y are star positions in pixel coordinates on the PC chip of WFPC2 based on the 2007 data. r is the cluster-centric distance in arcsecond. μ_x and μ_y are relative proper motions' components along the x and y directions of (PC) pixel coordinates (2007). V and I magnitudes are from the 1997 WFPC2 data.

TABLE 2

THE *VI* PHOTOMETRY AND RELATIVE PROPER MOTIONS OF THE MEMBER STARS ON THE WFC2 CHIP OF WPC2 (ONLINE TABLE 3).

No.	<i>X</i>	<i>Y</i>	<i>V</i>	<i>I</i>	<i>r</i> ($''$)	μ_x (mas/yr)	μ_y (mas/yr)
1	550.24	101.76	16.91	15.33	41.30	-0.08606	-0.16502
2	719.24	79.45	17.27	15.20	52.46	-0.16724	-0.10483
3	568.64	183.71	16.93	15.37	47.71	-0.38513	0.75699
4	306.83	94.90	18.51	16.65	28.67	-0.27374	0.03670
5	570.07	323.19	18.77	17.02	57.72	-0.17029	-0.17395
6	612.66	166.41	18.55	16.89	49.38	-0.61340	0.55496
7	435.92	216.66	18.86	17.19	43.29	-0.39001	0.47302
8	650.87	108.70	19.07	16.99	48.71	-0.26123	-0.25101
9	541.53	200.57	18.80	17.20	47.29	0.02197	0.55008
10	598.51	207.28	19.05	17.26	51.09	0.18921	0.39795
11	499.89	58.45	19.65	17.27	35.33	-0.27802	0.18848
12	434.89	60.65	19.10	17.42	31.46	0.00183	-0.51270
13	756.71	133.74	19.76	17.41	57.86	-0.00916	-0.22888
14	393.03	183.24	19.55	17.71	38.89	-0.01190	0.04791
15	380.83	193.30	20.50	17.65	39.28	-0.12695	-0.45609
16	618.54	158.25	19.45	17.79	49.27	0.16663	0.52109
17	505.67	257.21	20.14	18.02	49.58	0.06104	1.36597
18	557.61	125.01	19.97	18.08	43.22	-0.33203	-0.35904
19	598.44	292.96	20.93	18.08	56.99	0.12634	-0.16205
20	437.48	138.01	21.01	18.23	37.23	0.65094	-0.17105
21	377.79	105.99	21.01	18.38	32.04	0.60303	0.00603
22	424.70	137.99	20.55	18.65	36.62	0.30975	-0.25406
23	674.67	177.47	21.41	18.66	54.21	0.02136	0.27100
24	681.05	245.23	21.08	19.02	58.73	-0.41138	-0.16800
25	604.91	318.79	21.07	18.93	59.20	0.90515	-0.58594
26	323.33	77.77	20.63	18.77	27.70	-0.48920	-0.01053
27	447.54	136.91	21.77	18.87	37.65	0.25299	-0.75409
28	550.40	156.52	20.66	18.88	44.80	-0.88989	-0.81909
29	354.72	155.30	21.80	19.02	35.23	-0.15381	-0.12100
30	700.93	157.17	21.03	18.92	54.93	-0.15198	0.14694
31	577.11	280.32	20.84	19.18	54.93	-1.06690	-0.42877
32	330.58	53.92	20.89	19.09	25.96	-0.11383	0.53989
33	509.13	184.44	22.09	19.11	44.35	0.09705	0.12909
34	597.13	280.49	21.44	19.17	56.03	-0.52063	0.26398
35	633.55	263.40	21.21	19.03	56.95	0.27100	0.01221
36	605.45	234.53	21.67	19.42	53.33	-0.11597	-0.07095
37	360.84	84.45	22.25	19.40	29.61	0.30518	-0.04715
38	552.52	245.27	21.80	19.57	51.08	-0.27405	0.08804
39	661.16	257.19	21.98	19.76	58.23	-0.18921	-0.99121
40	337.96	98.91	22.62	19.77	29.95	0.10193	-0.12527
41	553.96	235.75	22.80	19.75	50.47	0.87585	-0.57800

□

TABLE 2—*Continued*

No.	X	Y	V	I	r (")	μ_x (mas/yr)	μ_y (mas/yr)
42	312.83	92.39	22.73	19.78	28.62	0.09308	-0.16891
43	475.60	66.45	22.58	19.74	34.28	0.67993	0.24353
44	747.63	165.59	22.27	19.88	58.77	0.02991	-0.74402
45	405.26	153.35	21.73	19.63	36.96	-1.03699	-0.68298
46	733.53	55.20	22.58	19.97	52.55	0.01953	0.67150
47	575.66	235.96	22.08	19.96	51.70	-0.54626	0.27206
48	525.22	64.82	22.96	19.94	37.40	-0.23804	-0.00397
49	403.81	141.45	23.17	20.14	35.95	0.52002	0.55801
50	369.42	57.80	22.98	20.08	27.87	-0.45715	0.67631
51	630.77	59.81	22.28	20.00	44.73	-0.23499	-0.75268
52	349.77	139.17	22.87	20.17	33.71	-0.41687	-0.29800
53	340.80	137.12	23.20	20.16	33.25	0.78400	-0.01892
54	326.88	61.06	22.59	19.75	26.42	-0.40802	0.31590
55	567.24	118.30	23.10	20.14	43.43	0.64819	0.08797
56	614.13	201.20	22.43	20.12	51.67	1.14258	-0.29999
57	741.31	83.13	22.14	20.14	54.35	-0.31433	-0.14107
58	424.91	55.56	23.41	20.32	30.54	-0.40100	-0.37369
59	466.82	133.40	23.64	20.27	38.39	0.97809	-0.24704
60	371.79	92.15	23.37	20.22	30.68	0.30304	-0.01244
61	492.06	97.91	22.82	20.27	37.36	1.08002	-0.36453
62	493.20	233.06	23.26	19.88	47.14	-0.70984	-0.05203
63	645.85	115.29	23.65	20.52	48.70	0.49988	0.19806
64	638.54	197.21	22.99	20.58	52.98	-0.16724	-0.45792
65	512.09	189.55	22.77	20.74	44.88	-0.47913	-0.62897
66	463.45	245.64	23.47	20.86	46.76	1.23108	0.32104
67	561.30	81.19	23.43	21.01	40.83	0.59326	-0.49355
68	695.94	94.14	23.45	21.14	51.34	0.00488	0.48660

X and Y are star positions in pixel coordinates on the PC chip of WFPC2 based on the 2007 data. r is the cluster-centric distance in arcsecond. μ_x and μ_y are relative proper motions' components along the x and y directions of (PC) pixel coordinates (2007). V and I magnitudes are from the 1997 WFPC2 data.

TABLE 3

THE *VI* PHOTOMETRY AND RELATIVE PROPER MOTIONS OF THE MEMBER STARS ON THE WFC4 CHIP OF WFPC2 (ONLINE TABLE 4).

No.	<i>X</i>	<i>Y</i>	<i>V</i>	<i>I</i>	<i>r</i> ($''$)	μ_x (mas/yr)	μ_y (mas/yr)
1	331.16	211.81	17.89	14.87	48.98	-0.07019	0.22003
2	194.24	169.76	17.31	15.33	36.84	-0.16998	0.34409
3	121.32	188.19	18.00	16.17	30.16	-0.44304	0.15900
4	331.39	242.91	18.56	16.51	49.10	-0.24994	0.64194
5	362.65	200.63	18.88	16.99	51.83	0.24292	0.54993
6	387.38	176.65	19.17	17.10	54.13	-0.12604	0.32410
7	188.60	71.17	18.86	17.32	38.24	0.39307	1.06903
8	317.60	345.95	19.42	17.26	49.32	0.57281	-0.01221
9	177.99	120.84	19.36	17.32	36.09	-0.55801	0.50400
10	69.27	78.94	19.48	17.46	28.00	-0.85289	-0.33165
11	165.81	225.45	19.40	17.50	34.13	-0.07401	0.05096
12	286.92	99.31	19.80	17.42	46.08	-0.10284	0.15472
13	446.87	215.81	19.75	17.62	59.40	-0.41992	0.69992
14	352.35	242.43	19.68	17.73	50.98	-1.16913	-0.14999
15	354.09	245.77	20.15	18.22	51.15	0.03998	-0.06592
16	285.43	299.33	20.23	18.15	45.59	0.15808	-0.47211
17	58.98	111.96	20.76	18.39	26.02	-0.23930	-0.26199
18	86.85	93.25	20.39	18.56	28.96	-0.78171	0.26367
19	158.24	100.59	21.44	18.77	34.83	0.14709	-0.45296
20	440.08	121.06	20.97	18.85	59.32	-0.16296	-0.30693
21	80.86	121.03	22.24	19.26	27.63	0.60005	-0.37399
22	377.99	92.63	21.35	19.25	54.23	-0.18524	-0.54657
23	226.03	153.90	21.07	19.28	39.84	-0.01404	0.52094
24	417.73	272.87	21.20	19.43	57.06	0.12390	-0.32196
25	267.39	275.64	22.75	19.60	43.65	0.21118	-0.44678
26	109.85	151.71	21.35	19.39	29.53	0.12604	-0.25513
27	250.84	135.20	21.49	19.45	42.29	-0.10712	-1.21704
28	226.51	76.14	22.13	19.73	41.35	-0.29190	-0.36797
29	386.56	203.95	22.28	20.12	53.97	0.29297	-1.01608
30	155.64	196.91	22.01	19.95	33.21	0.25696	-1.33789
31	397.20	142.06	22.92	20.25	55.26	1.11816	-0.46707
32	394.49	392.47	23.07	20.28	57.11	-0.54321	0.22980
33	288.93	111.01	23.02	20.45	46.05	0.16693	-1.11801

X and *Y* are star positions in pixel coordinates on the PC chip of WFPC2 based on the 2007 data. *r* is the cluster-centric distance in arcsecond. μ_x and μ_y are relative proper motions' components along the *x* and *y* directions of (PC) pixel coordinates (2007). *V* and *I* magnitudes are from the 1997 WFPC2 data.

ON THE ORIGIN OF MASS SEGREGATION IN NGC 3603

XIAOYING PANG¹, EVA. K. GREBEL

Astronomisches Rechen-Institut, Zentrum für Astronomie der Universität Heidelberg, Mönchhofstr. 12–14, 69120 Heidelberg, Germany

RICHARD J. ALLISON²

Institut für theoretische Astrophysik, Zentrum für Astronomie der Universität Heidelberg, Albert-Ueberle-Str. 2, 69120 Heidelberg, Germany

SIMON P. GOODWIN

Department of Physics and Astronomy, University of Sheffield, Sheffield S3 7RH, UK

MARTIN ALTMANN

Astronomisches Rechen-Institut, Zentrum für Astronomie der Universität Heidelberg, Mönchhofstr. 12–14, 69120 Heidelberg, Germany

DANIEL HARBECK

WIYN Observatory, 950 N. Cherry Ave, Tucson AZ 85719, USA

ANTHONY F.J. MOFFAT

Département de Physique, Université de Montréal, C.P. 6128, Succ. Centre-Ville, Montréal, QC H3C 3J7, and Centre de Recherche en Astrophysique du Québec, Canada

AND

LAURENT DRISSEN

Département de physique, de génie physique et d'optique, Université Laval, Québec QC G1V 0A6 and Centre de Recherche en Astrophysique du Québec, Canada

Draft version June 28, 2018

ABSTRACT

We present deep Hubble Space Telescope/Wide Field and Planetary Camera 2 photometry of the young HD 97950 star cluster in the giant H II region NGC 3603. The data were obtained in 1997 and 2007 permitting us to derive membership based on proper motions of the stars. Our data are consistent with an age of 1 Myr for the HD 97950 cluster. A possible age spread, if present in the cluster, appears to be small. The global slope of the incompleteness-corrected mass function for member stars within 60'' is $\Gamma = -0.88 \pm 0.15$, which is flatter than the value of a Salpeter slope of -1.35 . The radially varying mass function shows pronounced mass segregation ranging from slopes of -0.26 ± 0.32 in the inner 5'' to -0.94 ± 0.36 in the outermost annulus (40'' – 60''). Stars more massive than $50 M_{\odot}$ are found only in the cluster center. The Λ minimum spanning tree technique confirms significant mass segregation down to $30 M_{\odot}$. The dependence of Λ on mass, i.e., that high-mass stars are more segregated than low mass stars, and the (weak) dependence of the velocity dispersion on stellar mass might imply that the mass segregation is dynamical in origin. While primordial segregation cannot be excluded, the properties of the mass segregation indicate that dynamical mass segregation may have been the dominant process for segregation of high-mass stars.

Subject headings: H II regions: individual (NGC 3603) — open clusters and associations: individual (HD 97950) — stars: massive — stars: pre-main sequence — stars: luminosity function, mass function — stars: kinematics and dynamics

1. INTRODUCTION

The compact HD 97950 cluster in the luminous giant H II region NGC 3603 is one of the most massive young star clusters in the Milky Way. As the closest and densest starburst cluster accessible at optical wavelengths, it has been subject to many studies during the past few

decades. The cluster contains three Wolf-Rayet stars and up to 50 O-type stars (Drissen et al. 1995). Its total mass is estimated to be $\sim 10^4 M_{\odot}$ (Harayama et al. 2008) with an upper dynamical mass limit of $17600 \pm 3800 M_{\odot}$ (Rochau et al. 2010). The Wolf-Rayet stars show characteristics of WN6 stars, but also have Balmer absorption lines (Drissen et al. 1995), suggesting that these stars are actually core hydrogen-burning rather than evolved stars (Conti et al. 1995; de Koter, Heap, & Hubeny 1997). Two of these three WR stars are very close binaries (Schnurr et al. 2008).

xiaoying@ari.uni-heidelberg.de

¹ Fellow of the International Max-Planck Research School for Astronomy and Cosmic Physics at the University of Heidelberg and of the Heidelberg Graduate School for Fundamental Physics

² Alexander von Humboldt Research Fellow

Based on stellar spectral types, Melena et al. (2008) argue that the most massive stars in the HD 97950 cluster are coeval with ages of 1–2 Myr, while less massive stars (20–40 M_{\odot}) show a somewhat larger age spread of up to 4 Myr. Recent photometric studies have arrived at a range of ages ranging from an essentially single-burst population of 1 Myr (e.g., Sung & Bessell 2004; Stolte et al. 2004; Kudryavtseva et al. 2012) to 2 – 3 Myr (Eisenhauer et al. 1998; Harayama et al. 2008). The stars in the cluster outskirts may be slightly older (~ 5 Myr according to Sung & Bessell 2004), as is also suggested by spectroscopic studies of the late O and early B-type supergiants outside the core of the HD 97950 cluster (Melena et al. 2008). These evolved supergiants are probably not physically connected with HD 97950 owing to their advanced evolutionary state (e.g., Sher 25, see Brandner et al. 1997a, b) and higher age (Crowther et al. 2008; Melena et al. 2008). They may even indicate the occurrence of multiple episodes and possibly sequential star formation NGC 3603 (e.g., Moffat 1983; Melnick et al. 1989; De Pree et al. 1999; Tapia et al. 2001). Beccari et al. (2010) suggest an extended star formation episode of up to 10 – 20 Myr as indicated by an apparent age spread in pre-main-sequence stars in NGC 3603.

Despite its young age, the HD 97950 cluster shows pronounced mass segregation (e.g., Sung & Bessell 2004; Grebel & Gallagher 2004). Mass segregation is often observed in young star clusters (e.g., in the ONC, Hillenbrand & Hartmann 1998; Arches, Stolte et al. 2002; NGC 6611, Bonatto, Santos, & Bica 2006; NGC 2244 and NGC 6530, Chen et al. 2007; Schilbach et al. 2006), but the origin of mass segregation is still unclear. Bonnell & Davies (1998) argue that clusters cannot dynamically segregate in only a few Myr and so mass segregation in young clusters must be primordial.

Whether mass segregation is primordial or dynamical is an important constraint on theories of massive star formation and cluster formation and evolution. The competitive accretion theory (Bonnell et al. 2001; Bonnell & Bate 2006) suggests that protostars in the dense central regions of a young star cluster can accrete more material than those in the outskirts and that therefore primordial mass segregation would be a natural outcome of massive star formation. However, if mass segregation can occur dynamically on a very short timescale then massive star formation can occur anywhere in a cluster, possibly monolithically (e.g., Krumholz et al. 2009).

McMillan et al. (2007) show that young mass-segregated clusters may be the result of mergers between small clumps that are mass-segregated by either primordial or dynamical means. Allison et al. (2009a, 2010) suggest that observations support that clusters form with initial substructure, and show that for clusters with initially cool (subvirial) and clumpy distributions dynamical mass segregation can occur very rapidly in the cluster’s core after it has collapsed ($\sim 0.5 - 1$ Myr). In contrast to smooth, subvirial clusters, clumpy clusters collapse to much higher densities, enabling fast dynamical segregation.

The initial conditions of star clusters and the origin of mass segregation place important constraints on theories of massive star formation and cluster evolution. In the case of dynamical segregation, mass segregation is expected to be observable down to some “limiting mass”

that is proportional to the dynamical timescale (Allison et al. 2009a, 2010). This appears to be the case in, e.g., the Orion Nebula Cluster (ONC, ~ 1 Myr), which was found to be mass-segregated down to 5 M_{\odot} using the minimum spanning tree (MST) method (Allison et al. 2009b). Discussing the different methods commonly used to evaluate mass segregation in star clusters, Olczak et al. (2011) argue that the MST method is superior to the other methods since it does not make assumptions about symmetry or the location of the center of the distribution nor is it affected by uncertainties introduced by binning (see also Allison et al. 2009b; Küpper et al. 2011).

Here we analyze Hubble Space Telescope (HST) observations of the massive HD 97950 cluster in NGC 3603 obtained with the Wide-Field Planetary Camera 2 (WFPC2). In Section 2 we summarize the observations and data reduction. In Section 3 we discuss the color-magnitude diagram of the HD 97950 cluster. In Section 4 we infer the present-day mass function and discuss evidence for mass segregation based on the traditional mass function analysis in concentric annuli. Afterwards, we refine and quantify the mass segregation using an MST analysis. In Section 5, we investigate the origin of the mass segregation in the cluster with kinematic data (tangential velocity and velocity dispersion). We argue that dynamical processes are the dominant mechanism for the mass segregation in the cluster in Section 6. We present our conclusions and summary in Section 7.

2. OBSERVATIONS AND DATA REDUCTION

For our analysis of the HD 97950 cluster in NGC 3603 we used deep imaging data obtained with HST/WFPC2. The first observations were carried out in 1997 July (program GO 6763, PI: Drissen). The Planetary Camera (PC) chip was centered on the cluster. We obtained shallow, intermediate, and long exposures ranging from fractions of a second to 20 – 30 s in the *F547M* and *F814W* filters, respectively. Details are given in the exposure time log in Table 1. Earlier results from analyses of these data were presented by Sung & Bessell (2004) and by Grebel & Gallagher (2004).

The second data set was obtained in 2007 September (program GO 11193, PI: Brandner). The longest exposures lasted 100 s (*F555W*) and 160 s (*F814W*), considerably longer than in 1997 (Table 1). The ten-year epoch difference between the first and the second data set permits us to infer cluster membership using proper motions. Preliminary results of this analysis were presented by Pang et al. (2010). Rochau et al. (2010) published a proper motion study of the same dataset.

Both data sets were reduced using *HSTphot* (Dolphin 2000, 2005), a program developed for crowded-field stellar photometry of WFPC2 data. The shifts between the dithered images were determined following Koekemoer et al. (2002).

Stars at cluster-centric distances of $20'' - 60''$ are located on the three Wide Field Camera (WFC) chips in our data. While both in 1997 and in 2007 the PC chip was centered on the HD 97950 cluster, the two pointings are rotated by 51.4° with respect to each other. Thus the WFC chips only have 13% overlap, whereas the common area covered by the PC chip exposures from the two epochs amounts to $\sim 90\%$.

We only use images obtained in the filters either com-

mon to both datasets ($F814W$) or at comparable wavebands ($F547M$ in the 1997 dataset and $F555W$ in the 2007 dataset). Conveniently, $HSTphot$ transforms magnitudes in these filters into the V and I bands in the standard Johnson-Cousins system. We found 571 common stars on the PC and WFC chips within the cluster radius of $\sim 60''$ (Sung & Bessell 2004) observed in both epochs. The magnitudes of the common stars are taken from the 1997 photometry. The position- and magnitude-dependent incompleteness in the detection of point sources was assessed through artificial star experiments.

Proper motions were derived using common stars observed in the same filter during the two epochs in order to select likely cluster members and to weed out field stars. The membership of stars in the cluster is determined by fitting a two-Gaussian model to the proper motion distribution. We select only stars with membership probabilities larger than 0.7 to be cluster members (Jones & Walker 1988), which are retained in the subsequent analysis (see online Table 2-4). Fifty-nine stars on the PC and WFC chips (10% of the total number of common stars) were thus eliminated as foreground stars.

Because of the decreasing stellar density with increasing cluster radius the fractional foreground contamination increases with radius as well. Because of the high extinction in the NGC 3603 giant H II region, we may assume that background stars are effectively obscured and do not significantly contribute to our measurements. However, giant H II regions often show a complex age structure (e.g., Grebel & Chu 2000), and Beccari et al. (2010) found older PMS stars in a wide area around the cluster. Hence we cannot exclude the presence of older stars belonging to NGC 3603 that would be difficult to disentangle from younger cluster stars at the same distance via proper motions.

3. COLOR-MAGNITUDE DIAGRAMS AND AGE

Figure 1 shows the color-magnitude diagrams (CMDs) of the HD 97950 cluster including all common stars measured in the two epochs in the cluster core (PC: $20''$, left panel) and within the cluster radius ($\sim 60''$, Sung & Bessell 2004; PC & WFCs, right panel). The CMDs show a steep main sequence (MS) on the PC and a broader MS (at the faint end) when the WFCs are included. The contamination of foreground stars is more severe for the WFCs (grey dots) since they cover a larger area. There is a broad region of redder pre-main-sequence (PMS) stars and a wide transition region between the MS and the PMS in both CMDs. Like Harayama et al. (2008), we do not see clear evidence of a sequence of equal-mass binaries as earlier suggested by Stolte et al. (2004).

Figure 5 in Sung & Bessell (2004) shows that $E(B-V)$ stays unchanged with 1.25 mag within $30''$ (see also Mofat 1983). We adopt a reddening law of $E(V-I)/E(B-V) = 1.45 \pm 0.05$ and $E(B-V) = 1.25$ from Sung & Bessell (2004), and assume a uniform extinction of $A_V = 4.44 \pm 0.15$ ($R_V = 3.55$) throughout the region within $r \leq 60''$. The reddening corrected MS on the PC aligns with that on the WFCs (right panel of Figure 1), indicating that our adoption is reasonable.

In order to derive stellar masses along the main sequence, we use the isochrone models of Lejeune & Schaerer (2001). These isochrones extend to masses

above $100 M_\odot$, appropriate for the HD 97950 cluster (see Schnurr et al. 2008; Crowther et al. 2010). For the PMS stars on WFPC2 images, for which the mass goes down to $0.8 M_\odot$ (Drissen 1999), we use Siess et al. (2000) isochrones, which cover a larger mass range ($0.1-7.0 M_\odot$) than other PMS isochrones. We adopt a distance of $d = 6.9 \pm 0.6$ kpc from Sung & Bessell (2004) and solar metallicity for the HD 97950 cluster (see Hendry et al. 2008) throughout this paper.

The MS of HD 97950 is well-represented by a Lejeune & Schaerer 1 Myr isochrone (Figure 1). Slightly older MS isochrones also provide a good fit, in agreement with spectroscopic age estimates for the massive stars. The Siess isochrones along the PMS locus indicate an age spread of up to 3 Myr. The color uncertainties of the bulk of our PMS stars (fainter than $V = 19$) are still smaller than the width of the color distribution in that area, which may be in part caused by differential reddening (Pang et al. 2011). In the “turn-on” region where PMS stars join the MS we find a broad range of luminosities ($16 \lesssim V \lesssim 19$), which either again indicates an age spread or is due to the presence of (MS) stars with surviving circumstellar disks (Stolte et al. 2004).

Non-accreting isochrones, e.g., the Siess isochrones, tend to overestimate the stellar ages for stars whose effective temperature is above 3500 K (Hosokawa et al. 2011). Baraffe et al. (2009) suggest that the apparent spread of the PMS stars in the Hertzsprung-Russell diagram at ages of a few Myr can be plausibly attributed to a spread in the stellar radius and a different episodic accretion history, instead of an age range as inferred from non-accreting stellar evolutionary models (e.g., Siess 2000).

The recent study of massive MS stars in the HD 97950 cluster by Kudryavtseva et al. (2012) finds that the age spread is as small as 0.1 Myr. A few low-mass MS stars at $V > 20$ (within $r > 20''$; right panel in Figure 1) are below the region where most of the cluster MS stars are located (see also Grebel & Gallagher 2004). Considering their small proper motions, these faint MS stars are consistent with being cluster members, which would corroborate an age spread in the cluster as suggested in a number of earlier studies (see Section 1). Alternatively, they might be stars from earlier star formation in the wider NGC 3603 H II region that we observe superimposed at the cluster’s location. That would be consistent with the much more widely distributed population of older PMS stars around the HD 97950 cluster described by Beccari et al. (2010).

Considering the above findings and deliberations, we excluded the MS stars at $V > 20$ from the age determination for the HD 97950 cluster. We conclude that an age spread (if any) in the HD 97950 cluster must be small. We therefore adopt an age of 1 Myr for the cluster.

4. THE MASS FUNCTION AND MASS SEGREGATION

4.1. *The qualitative approach: Mass function determination in cluster-centric annuli*

In order to derive the mass function of the HD 97950 cluster, we count stars in absolute V -magnitude bins spaced such that they cover mass bins with a logarithmic size of 0.2. Using the same procedure as Grebel & Chu (2000), we find the absolute magnitudes corresponding to mass bins along the earlier described isochrones assuming

an age of 1 Myr. We applied a color cut of $(V - I) = 2.4$ to separate MS and PMS stars.

Since the crowding is severe in the central region of the HD 97950 cluster, we corrected the count rates for incompleteness depending on their positions and magnitudes. We display the completeness dependence on stellar mass for the PC chip in Figure 2. In the outer annulus ($r > 15''$), stars above $1.5 M_{\odot}$ are more than 50% complete. As the crowding becomes stronger towards the cluster center, in the region within $r < 5''$ only stars more massive than $4 M_{\odot}$ are $> 50\%$ complete. Therefore, many faint stars in the central region remain undetected. A completeness test is also run for median and deep exposure images of WFC chips in which crowding effects might intervene. However, since the stars on the WFC chips ($\sim 60''$) are quite far from the cluster core, they are not significantly affected by crowding. Their completeness fraction does not depend on the cluster-centric distance (see Figure 3).

The three luminous Wolf-Rayet stars near the center of the HD 97950 cluster are saturated in our WFPC2 photometry. Therefore they were added by hand to the highest mass bin using the masses and magnitudes of Schnurr et al. (2008). Since there are very few MS stars fainter than $V = 20$ mag in the core of the cluster (left panel in Figure 1), the presence of a small number of stars along the lower MS ($V > 20$ mag) at larger cluster-centric distances (right panel in Figure 1) may be attributed to earlier generations (Section 3). Consequently, we exclude stars with $V > 20$ mag and $(V - I) < 2.4$ from our mass function derivation.

Even though the overlap between the WFC chip exposures obtained in 1997 and 2007 is small, we can attempt to increase the area available for analysis by also including those WFC stars in regions that do not overlap. This greatly reduces the corrections for missing area. While this will permit us to consider the mass function within the entire cluster radius ($\sim 60''$; Sung & Bessell 2004), it also requires statistical field star subtraction. This approach is viable for a classical mass function analysis in which we consider the mass function within different cluster-centric annuli, but the subsequent MST analysis is necessarily limited to the inner $20''$ covered by the PC chip, since the MST method requires a contiguous area.

We count the total number of incompleteness-corrected, proper-motion-selected foreground stars in the PC and the WFC chips in each magnitude bin considered. Assuming that foreground stars are essentially homogeneously distributed across the entire area covered by the WFPC2 exposures, this approach provides us with the best possible statistics for foreground stars. We obtain the number of foreground stars per magnitude bin and per unit area. In order to correct for field star contamination, we then only need to subtract these numbers after scaling them by the area actually considered within a given annulus.

Fitting the corrected number counts of all probable MS and PMS stars within a mass range of $\sim 1 - 100 M_{\odot}$ results in a mass function slope of $\Gamma = -0.82 \pm 0.20$ for the PC chip. Our result is in agreement with the earlier WFPC2 study of Sung & Bessell (2004) within error, who obtained $\Gamma = -0.9 \pm 0.1$ for stars on the PC chip. Combining the corrected number counts of all stars within $60''$, the resulting slope of the global mass function

is $\Gamma = -0.88 \pm 0.15$ ($\log(\text{mass}/M_{\odot}) > 0.6$), which is flatter than a Salpeter slope of -1.35 .

In Figure 4 we also show the mass function of the HD 97950 cluster in different concentric annuli out to $60''$. Two effects stand out: (1) the slope of the mass function increases with radius, and (2) the more massive stars are concentrated in the center and are missing at larger radii.

Our photometric mass function is affected by the uncertainties in the isochrone models used to derive the masses of cluster member stars. One such uncertainty is the unknown amount of stellar rotation that can affect the colors and magnitudes of stars (Grebel et al. 1996). The stellar evolution models with rotation (Ekström et al. 2012) generate a slightly narrower MS width than non-rotating models (e.g., Schaller et al. 1992), and predict larger final masses at the end of evolution for stars with initial masses in the range of $45-100 M_{\odot}$. Thus a flatter slope of mass function will result.

Another uncertainty is unrecognized binarity. Here we implicitly make the simplified assumption that we are dealing with non-rotating, single stars as discussed in Section 3. Also, we neglect a possible age spread in the cluster, but emphasize that a small spread such as the spectroscopically inferred age spread of $1 - 2$ Myr for massive MS stars does not affect the photometrically estimated masses significantly. Moreover, the above analysis of mass segregation in HD 97950 is sensitive to the determination of the position of the cluster center, and the number and size of the radial bins used (e.g., Gouliermis et al. 2004).

4.2. The quantitative approach: Mass segregation determination via the minimum spanning tree

In order to quantify the mass segregation, we apply the Λ -method (Allison et al. 2009b; Parker et al. 2011) to the MS members ($> 3.5 M_{\odot}$) on the PC chip. We only consider MS stars since lower-mass stars (primarily PMS stars) are incomplete in the center due to crowding effects. We take a subset of n stars of similar mass (the 1st to n th most massive stars, or the $(n + 1)$ th to $2n$ th most massive stars for example) and find the length of the MST that connects those stars with the shortest path without closed loops. We then take a large number of random sets of n stars of *any* mass and obtain the median and the 1/6th and 5/6th percentiles to obtain a (possibly asymmetric) 1σ error (the vertical bar in Figure 5). A subset is mass-segregated if Λ (the ratio of the MST length of random stars over massive stars) is larger than unity, i.e., the stars in that subset are more concentrated in their distribution than a random sample (see Allison et al. 2009b; Maschberger & Clarke 2011; Parker et al. 2011).

Figure 5 shows the values of Λ for samples of 20 stars moving in steps of 10 stars (therefore every second data-point is uncorrelated with each other). The first 20 stars all have masses $> 35 M_{\odot}$, and the second mass bin is in the range $27 - 45 M_{\odot}$. The first two bins have a Λ significantly greater than unity – i.e., they are more concentrated than random stars. Varying the size of bins always shows a significant degree of mass segregation for masses $> 30 M_{\odot}$. Considering error bars, the degree of segregation among stars with masses $< 30 M_{\odot}$ is not pronounced.

We note that two bins just below $20 M_{\odot}$ also show some evidence of mass segregation. This is due to a close pair of stars of very similar mass ($\sim 18 M_{\odot}$).

5. ORIGIN OF THE MASS SEGREGATION

We note that (a) the HD 97950 cluster is strongly mass-segregated above $30 M_{\odot}$, and (b) all other masses of stars are randomly distributed throughout the cluster (Figure 4 & 5). As we shall argue, this strongly suggests a dynamical origin for mass segregation in HD 97950. To verify this, we explore the kinematics of the cluster via proper motions. Since the faint stars are incomplete especially in the cluster center, in order not to bias our result, we only use stars that are more than 50% complete, which corresponds to stars brighter than $V = 18$ mag within the inner $5''$ region and stars brighter than $V = 22$ mag in the region $> 5''$ from the cluster center.

5.1. Tangential velocity profile

We convert the proper motions of stars into tangential velocities and show their distributions in Figure 6. The vertical bar is the tangential velocity dispersion for stars in each magnitude bin or annulus. The (mean) tangential velocity V_t increases slightly from bright to faint stars (upper panel), and from the inner to the outer part of the cluster (lower panel). However, owing to the large scatter, the ascending trend is not significant.

The tangential velocity dispersion for stars $> 30 M_{\odot}$ is $6.8 \pm 0.8 \text{ km s}^{-1}$. It does not change much for stars of $10 M_{\odot}$ ($5.9 \pm 0.6 \text{ km s}^{-1}$), but increases to $9.0 \pm 0.9 \text{ km s}^{-1}$ for stars of $\sim 2.5 M_{\odot}$. Since the energy equipartition is mass-dependent (see Section 5.3), dynamical segregation may only manifest itself among the few most massive stars, considering the young age of the cluster. This might indicate that equipartition is not taking place in the entire cluster yet (Rochau et al. 2010). However, accounting for the observational uncertainties (see Section 5.2), the dependence of velocity dispersion on stellar mass is weak, similar to the finding of Rochau et al. (2010).

5.2. Velocity dispersion

We compute the observed one-dimensional dispersion of proper motions of member stars on the PC chip, which centers at the cluster and provides a more reliable velocity dispersion than the WFC chips due to the higher spatial resolution. We compute the observed one-dimensional dispersion (OD) of the proper motions of member stars: $\sigma_{x,obs} = 0.316 \pm 0.014 \text{ mas yr}^{-1}$ and $\sigma_{y,obs} = 0.325 \pm 0.014 \text{ mas yr}^{-1}$ (x and y are pixel coordinates). We assume that the error of the observed dispersion is given by the measurement uncertainty, consisting of random errors from single epoch observations (1997 and 2007) and centroid offsets.

To compute the positional random errors of the observations, we divide the original single epoch data (1997 & 2007) into two subsamples, respectively. After doing photometry on each subsample, we find the common stars ($V < 18$ mag within $5''$ from the cluster center and $V < 22$ mag for regions $> 5''$) between the two subsets of the same epoch. The detected positions of the same star in the two subsamples tend to be slightly offset

from one another. The standard deviation of this positional offset is the random error, which amounts to $\sigma_{x,r} = 0.262 \pm 0.007 \text{ mas yr}^{-1}$ and $\sigma_{y,r} = 0.233 \pm 0.008 \text{ mas yr}^{-1}$ when considering the contributions from both observing epochs.

We evaluate the quality of the centroids of the detected stars by comparing their positions in images obtained in the same filter and with the same exposure time in the same epoch. The average intra-filter offsets are $\sigma_{x,cent} \sim 0.10 \text{ mas yr}^{-1}$ and $\sigma_{y,cent} \sim 0.11 \text{ mas yr}^{-1}$. We subtract the random errors and centroid offsets from the observed dispersion and obtain the absolute one-dimensional velocity dispersions: $\sigma_x = 0.146 \pm 0.016 \text{ mas yr}^{-1}$ and $\sigma_y = 0.198 \pm 0.016 \text{ mas yr}^{-1}$. By adopting a distance of $d = 6.9$ kpc from Sung & Bessell (2004), the one-dimensional velocity dispersions are $\sigma_{x,c} = 4.8 \pm 0.5 \text{ km s}^{-1}$ and $\sigma_{y,c} = 6.5 \pm 0.5 \text{ km s}^{-1}$. The uncertainty, $\sqrt{\text{var}(\sigma_{x/y,c})}$, is computed according to Equation 12 in Pryor & Meylan (1993):

$$\text{var}(\sigma_{x/y,c}) = (\sigma_{x/y,c}^2 + \sigma_{x/y,e}^2) / (2N\sigma_{x/y,c}^2) \quad (1)$$

where $\sigma_{x/y,c}$ is the real one-dimensional dispersion and $\sigma_{x/y,e}$ the measurement uncertainty (random errors and centroid offsets).

5.3. Dynamical mass of the cluster

Harayama et al. (2008) derived the half-mass radius of NGC 3603 to be $R_{hm} \sim 0.7 \text{ pc}$ from low-mass stars with masses of ~ 0.5 to $\sim 2.5 M_{\odot}$. As stars above $30 M_{\odot}$ are significantly segregated in the center (Section 4), the true cluster half-mass radius would be smaller. We adopted a half-mass radius of 0.5 pc (Rochau et al. 2010). The dynamical mass M_{dyn} of the HD 97950 cluster can be calculated from Spitzer's (1987) formula using the one-dimensional dispersion we derived ($4.8 - 6.5 \text{ km s}^{-1}$):

$$M_{dyn} \sim \eta \frac{R_{hm} \sigma_{vt}^2}{G}$$

η is a dimensionless parameter in the equation. The square of the three-dimensional velocity dispersion is three times larger than the square of the one-dimensional dispersion, σ_{vt}^2 . Moreover, we are taking a factor of $4/3$ from the projection of half-light radius on the sky into account. Furthermore, there is a factor of $5/2$ from the conversion to a star cluster fitted with a King mass profile. Thus η is about 10.0 (see Fleck et al. 2006 for details). Observers usually use $\eta=9.75$ when working with the half-mass radius R_{hm} instead of the half-light radius.

This results in a dynamical mass of $M_{dyn} \sim 1.9 \pm 0.6 \times 10^4 M_{\odot}$ ($\eta = 9.75$). This mass is close to the photometric mass $M_{phot} = 1 - 1.6 \times 10^4 M_{\odot}$ derived from observations of the stellar content (Harayama et al. 2008), which might suggest NGC 3603 is more or less virialized. Several other young star clusters are also found to be virialized with comparable photometric and dynamical masses, e.g., Westerlund 1: Cottaar et al. (2012); R 136, Bosch et al. (2009); ONC, Jones & Walker (1988), Tobin et al. (2009).

Compared to the previous study of Rochau et al. (2010) of NGC 3603 with the same dataset, our study differs from theirs in the following aspects: (1) The velocity

dispersion we derived is based on member stars with a completeness of more than 50%. These are stars brighter than $V = 18$ mag within $5''$ from the center and stars brighter than $V = 22$ mag in the annulus $5'' - 20''$. Rochau et al. (2010) computed the velocity dispersion for intermediate-mass stars ($1.7 - 9.0 M_{\odot}$) in the magnitude range of $16 < V < 20$ mag within $15''$. As the photometric uncertainty increases towards fainter stars, this might explain why Rochau et al. (2010) arrived at a smaller value ($4.5 \pm 0.8 \text{ km s}^{-1}$) for the velocity dispersion. (2) The sinusoidal pixel phase error and breathing error on the pixel scale are smaller than the astrometric uncertainty of HSTphot (0.03 pixels). Therefore we did not subtract these two error sources which are considered in Rochau et al. (2010). Nevertheless, the dynamical mass of our study and that of Rochau et al. (2010) ($17600 \pm 3800 M_{\odot}$) agree with each other within the errors.

6. DYNAMICAL SEGREGATION IN THE CLUSTER CORE

Very similar patterns of mass segregation have been observed in the two other clusters analyzed with the Λ -method: the ONC (Allison et al. 2009b) and Trumpler 14 (Sana et al. 2010). Allison et al. (2009a) proposed a dynamical origin for mass segregation due to two-body relaxation in a dense phase to explain the ONC. They proposed that the ONC underwent a short-lived dense phase in which the two-body relaxation time was very short.

The two-body relaxation time t_{relax} of a system is given by

$$t_{\text{relax}} \sim \frac{N}{8 \ln N} t_{\text{cross}}$$

where N is the number of stars in the cluster, and t_{cross} is the crossing time of the system. Dynamical mass segregation occurs due to the equipartition of energies in two-body encounters. The rate at which a star will approach equipartition depends on the mass of that star, M , relative to the average mass of stars in the system, $\langle m \rangle$. The time to segregate t_{seg} down to a mass M is

$$t_{\text{seg}}(M) \sim \frac{\langle m \rangle}{M} t_{\text{relax}} = \frac{\langle m \rangle}{M} \frac{N}{8 \ln N} t_{\text{cross}}. \quad (2)$$

Allison et al. (2009a) showed that for a dense phase that lasts one crossing time the ONC should mass-segregate down to $5 M_{\odot}$, but not below, which is what is observed.

In Allison et al.'s (2009a) simulation, they find that in the core the segregation time is similar to the crossing time. To extend their argument to the HD 97950 cluster, we need to input the total stellar number N and mean stellar mass $\langle m \rangle$ into equation (2). Nürnberger et al. (2002) found about 10216 bona-fide stars to construct the luminosity function of the HD 97950 cluster from infrared observations. We adopted their result and assume a total number of stars, $N = 10^4$, and a mean stellar mass of $\langle m \rangle = 0.4 M_{\odot}$ from Kroupa et al.'s (2002) initial mass function. Inserting $N = 10^4$ and $\langle m \rangle = 0.4 M_{\odot}$ into equation (2) suggests that in one crossing time the HD 97950 cluster should mass-segregate to a mass of $30 M_{\odot}$. This is exactly what is observed in the core of the cluster. The highest-mass stars are sinking further into the core of the cluster, and are found to be more mass-segregated than lower-mass stars (Figure

5). Higher-mass stars are more efficient at this process and thus mass-segregate faster. That the stars in the HD 97950 cluster show the same dependence on mass as do purely dynamical and initially non-mass-segregated N -body simulations (Allison et al. 2009a, 2010) indicates that dynamical mass segregation may be the dominant process for the mass segregation in the cluster. Furthermore, no formation process (e.g., competitive accretion) is known to produce mass segregation down to one particular mass. Recent infrared observations by Gvaramadze et al. (2012) and Roman-Lopes (2012) find a (bow-shock-producing) massive star and a massive binary in the vicinity of NGC 3603, which are suggested to have been ejected from the cluster HD 97950 via a three-body encounter. These observations may imply that vivid dynamical evolution is already taking place inside the cluster.

We also note that binaries may shorten the relaxation time and accelerate segregation. But at the same time, primordial binaries increase the chance of ejections of OB stars (Portegies Zwart et al. 2010), working against the observed mass segregation in the HD 97950 cluster. As no binary sequence can be seen in Figure 1, we cannot quantify the presence of binaries in the cluster and their effects on the mass segregation.

7. SUMMARY

We analyzed broad-band HST/WFPC2 imaging of the HD 97950 star cluster obtained in 1997 and in 2007. We used the epoch difference to establish a proper-motion-selected sample of probable cluster members. The main results of our subsequent analysis are:

1. We find pronounced mass segregation in the cluster, as did previous studies. The slope of the mass function, measured within concentric annuli around the cluster center, varies radially from -0.26 ± 0.32 within $5''$ from the center to -0.94 ± 0.36 in an annulus of $40'' - 60''$ around the center. Very massive stars are only found near the cluster center and are not observed at larger radii. The global slope of the mass function for member stars on the PC chip is $\Gamma = -0.82 \pm 0.20$. It stays almost unchanged at a value of $\Gamma = -0.88 \pm 0.15$ for all stars ($\log(\text{mass}/M_{\odot}) > 0.6$) within the cluster radius of $\sim 60''$ (Sung & Bessell 2004), which is flatter than a Salpeter slope.

2. Using the Λ MST method, we find the HD 97950 cluster to be significantly mass-segregated down to $30 M_{\odot}$. The most massive stars are the most mass-segregated ones. A simple extension of the Allison et al. (2009a) dynamical model for mass segregation in the ONC suggests that HD 97950 should be mass-segregated to $30 M_{\odot}$, in very good agreement with the observations. Furthermore, we find a weak dependence of the tangential velocity dispersion on the stellar mass. The tangential velocity dispersion increases from $6.8 \pm 0.8 \text{ km s}^{-1}$ for stars $> 30 M_{\odot}$ to $9.0 \pm 0.9 \text{ km s}^{-1}$ for stars of $\sim 2.5 M_{\odot}$. Considering the uncertainty, this suggests that energy equipartition does not affect the whole cluster yet, but so far only the most massive stars of the HD 97950 cluster.

3. We compute a dynamical mass of $M_{\text{dyn}} \sim (1.9 \pm 0.6) \times 10^4 M_{\odot}$ for the HD 97950 cluster in NGC 3603, which is close to its photometric mass (Harayama et al. 2008). This may imply that the cluster is in a state of

virialization, similar to other young massive clusters.

We thank Rainer Spurzem and Siegfried Röser for helpful discussions. X.P. acknowledges support within the framework of the Excellence Initiative by the German Research Foundation (DFG) through the Heidelberg Graduate School of Fundamental Physics (grant number GSC 129/1). This work was partially supported by Sonderforschungsbereich 881 “The Milky Way System” of the German Research Foundation (subproject B5). LD and AFJM are grateful for financial assistance from NSERC (Canada) and FQRNT (Quebec).

REFERENCES

- Allison, R. J., Goodwin, S. P., Parker, R. J., de Grijs, R., Portegies Zwart, S. F., & Kouwenhoven, M. B. N. 2009a, *ApJ*, 700, L99
- Allison, R. J., Goodwin, S. P., Parker, R. J., Portegies Zwart, S. F., de Grijs, R., & Kouwenhoven, M. B. N. 2009b, *MNRAS*, 395, 1449
- Allison, R. J., Goodwin, S. P., Parker, R. J., Portegies Zwart, S. F., & de Grijs, R. 2010, *MNRAS*, 407, 1098
- Baraffe, I., Chabrier, G., & Gallardo, J. 2009, *ApJ*, 702, L27
- Beccari, G., et al. 2010, *ApJ*, 720, 1108
- Bonatto, C., Santos Jr, J. F. C., Bica, E. 2006, *A&A*, 445, 567
- Bonnell, I. A., & Davies, M. B. 1998, *MNRAS*, 295, 691
- Bonnell, I. A., & Bate, M. R. 2006, *MNRAS*, 370, 488
- Bonnell, I. A., Clarke, C. J., Bate, M. R., & Pringle, J. E. 2001, *MNRAS*, 324, 573
- Bosch, G., Terlevich, E., & Terlevich, R. 2009, *AJ*, 137, 3437
- Brandner, W., Grebel, E. K., Chu, Y.-H., & Weis, K. 1997a, *ApJ*, 475, L45
- Brandner, W., Chu, Y.-H., Eisenhauer, F., Grebel, E. K., & Points, S. D. 1997b, *ApJ*, 489, L153
- Chen, L., de Grijs, R., & Zhao, J. L. 2007, *AJ*, 134, 1368
- Cottaar, M., Meyer, M. R., Andersen, M., & Espinoza, P. 2012, *AAP*, 539, A5
- Crowther, P. A., Schnurr, O., Hirschi, R., Yusof, N., Parker, R. J., Goodwin, S. P., & Kassim, H. A. 2010, *MNRAS*, 408, 731
- Crowther, P. A., & Dessart, L. 1998, *MNRAS*, 296, 622
- Crowther, P. A., Lennon, D. J., Walborn, N. R., & Smartt, S. J. 2008, in *ASP Conf. Ser.* 388, *Mass Loss from Stars and the Evolution of Stellar Clusters*, ed. A. de Koter, L. J. Smith, & L. B. F. M. Waters, (San Francisco, CA: ASP), 109
- de Koter, A., Heap, S. R., & Hubeny, I. 1997, *ApJ*, 477, 792
- De Pree, C.G., Nysewander, M.C., & Goss, W.M. 1999, *AJ*, 117, 2902
- Dolphin, A. E. 2000, *PASP*, 112, 1397
- Dolphin, A. E. 2005, *HSTphot User’s Guide*, <http://purcell.as.arizona.edu/hstphot/>
- Drissen, L., Moffat, A. F. J., Walborn, N. R., & Shara, M. M. 1995, *AJ*, 110, 2235
- Drissen, L. 1999, in *IAU Symp.* 193, *Wolf-Rayet Phenomena in Massive Stars and Starburst Galaxies*, ed. van der Hucht, K. A., Koenigsberger, G., & Eenens, P. R. J. (San Francisco: ASP), 403
- Eisenhauer, F., Quirrenbach, A., Zinnecker, H., & Genzel, R. 1998, *ApJ*, 498, 278
- Ekström, S., Georgy, C., Eggenberger, P., et al. 2012, *A&A*, 537, A146
- Fleck, J.-J., Boily, C. M., Lançon, A., & Deiters, S. 2006, *MNRAS*, 369, 1392
- Grebel, E. K., & Chu, Y.-H. 2000, *AJ*, 119, 787
- Grebel, E. K., & Gallagher, J. S. 2004, in *ASP Conf. Ser.* 322, *The Formation and Evolution of Massive Young Star Clusters*, ed. H. J. G. L. M. Lamers, L. J. Smith, & A. Nota (San Francisco, CA: ASP), 101
- Grebel, E. K., Roberts, W. J., & Brandner, W. 1996, *A&A*, 311, 470
- Gouliermis, D., Keller, S. C., Kontizas, M., Kontizas, E., & Bellas-Velidis, I. 2004, *A&A*, 416, 137
- Gvaramadze, V. V., Kniazev, A. Y., Chene, A.-N., & Schnurr, O. 2012, arXiv:1211.5926
- Harayama, Y., Eisenhauer, F., & Martins, F. 2008, *ApJ*, 675, 1319
- Hendry, M. A., Smartt, S. J., Skillman, E. D., Evans, C. J., Trundle, C., Lennon, D. J., Crowther, P. A., & Hunter, I. 2008, *MNRAS*, 388, 1127
- Hillenbrand, L.A., Hartmann, L.E. 1998, *ApJ*, 492, 540
- Hosokawa, T., Offner, S. S. R., & Krumholz, M. R. 2011, *ApJ*, 738, 140
- Jones, B. F., & Walker, M. F. 1988, *AJ*, 95, 1755
- Koekemoer, A. M., et al. 2002, “HST Dither Handbook”, Version 2.0 (Baltimore: STScI)
- Kroupa, P. 2002, *Science*, 295, 82
- Krumholz, M. R., Klein, R. I., McKee, C. F., Offner, S. S. R., Cunningham, A. J. 2009, *Science*, 323, 754
- Kudryavtseva, N., Brandner, W., Gennaro, M., et al. 2012, *ApJ*, 750, L44
- Küpper, A. H. W., Maschberger, T., Kroupa, P., & Baumgardt, H. 2011, *MNRAS*, 417, 2300
- Lejeune, T., & Schaerer, D. 2001, *A&A*, 366, 538
- Maschberger, T., & Clarke, C. J. 2011, *MNRAS*, 416, 541
- McMillan, S. L. W., Vesperini, E., & Portegies Zwart, S. F. 2007, *ApJ*, 655, L45
- Melena, N. W., Massey, P., Morrell, N. I., & Zangari, A. M. 2008, *AJ*, 135, 878
- Melnick, J., Tapia, M., & Terlevich, R. 1989, *A&A*, 213, 89
- Moffat, A. F. J. 1983, *A&A*, 124, 273
- Nürnberg, D. E. A., & Petr-Gotzens, M. G. 2002, *A&A*, 382, 537
- Olczak, C., Spurzem, R., & Henning, T. 2011, *A&A*, 532, A119
- Pang, X., Grebel, E. K., & Altmann, M. 2010, in *IAU Symp.* 266, *Star clusters: basic galactic building blocks throughout time and space*, ed. de Grijs & J. R. D. Lépine (Cambridge: CUP), 24
- Pang, X., Pasquali, A., & Grebel, E. K. 2011, *AJ*, 142, 132
- Parker, R. J., Bouvier, J., Goodwin, S. P., et al. 2011, *MNRAS*, 412, 2489
- Portegies Zwart, S. F., McMillan, S. L. W., & Gieles, M. 2010, *ARA&A*, 48, 431
- Rochau, B., Brandner, W., Stolte, A., Gennaro, M., Gouliermis, D., Da Rio, N., Dzyurkevich, N., & Henning, T. 2010, *ApJ*, 716, L90
- Roman-Lopes, A. 2012, *MNRAS*, 427, L65
- Sana, H., Momany, Y., Gieles, M., et al. 2010, *AAP*, 515, A26
- Schaller, G., Schaerer, D., Meynet, G., & Maeder, A. 1992, *A&AS*, 96, 269
- Schilbach, E., Kharchenko, N. V., Piskunov, A. E., Röser, S., & Scholz, R.-D. 2006, *A&A*, 456, 523
- Schnurr, O., Casoli, J., Chené, A.-N., Moffat, A. F. J., & St-Louis, N. 2008, *MNRAS*, 389, L38
- Siess, L., Dufour, E., & Forestini, M. 2000, *A&A*, 358, 593
- Spitzer, L., Jr. 1987, *Dynamical Evolution of Globular Clusters*, Princeton University Press
- Stolte, A., Grebel, E. K., Brandner, W., & Figer, D. F. 2002, *A&A*, 394, 459
- Stolte, A., Brandner, W., Brandl, B., Zinnecker, H., & Grebel, E. K. 2004, *AJ*, 128, 765
- Sung, H., & Bessell, M. S. 2004, *AJ*, 127, 1014
- Tapia, M., Bohigas, J., Pérez, B., Roth, M., & Ruiz, M.T. 2001, *RMxAA*, 37, 39
- Tobin, J. J., Hartmann, L., Furesz, G., Mateo, M., & Megeath, S. T. 2009, *ApJ*, 697, 1103

Table 1
Exposure time log of the HST/WFPC2 observations of the HD 97950 cluster

Filter	Shallow Exposures [s]	No. of Frame	Median Exposures [s]	No. of Frame	Deep Exposures [s]	No. of Frame
1997						
<i>F547M</i>	1	3	10	12	30	8
<i>F814W</i>	0.4	3	5	12	20	8
2007						
<i>F555W</i>	0.4	4	26	4	100	4
<i>F814W</i>	–	–	18	4	160	4

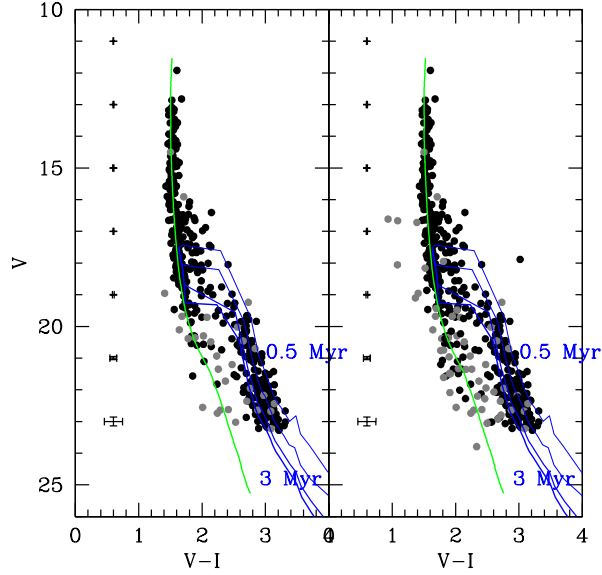


Figure 1. CMDs of all common stars found in the 1997 and 2007 WFPC2 data (left: within 20'', PC; right: within 60'', PC & WFC chips). Proper-motion members of the HD 97950 cluster are shown as black dots. Probable non-members are indicated as grey dots. The vertical solid green line is a 1 Myr MS isochrone for solar abundance from Lejeune & Schaerer (2001). The blue lines are PMS isochrones from Siess et al. (2000). From right to left (increase of thickness of the lines) isochrones for 0.5, 1, 2, 3 Myr are plotted. Representative mean errors of magnitude and color are indicated on the left.

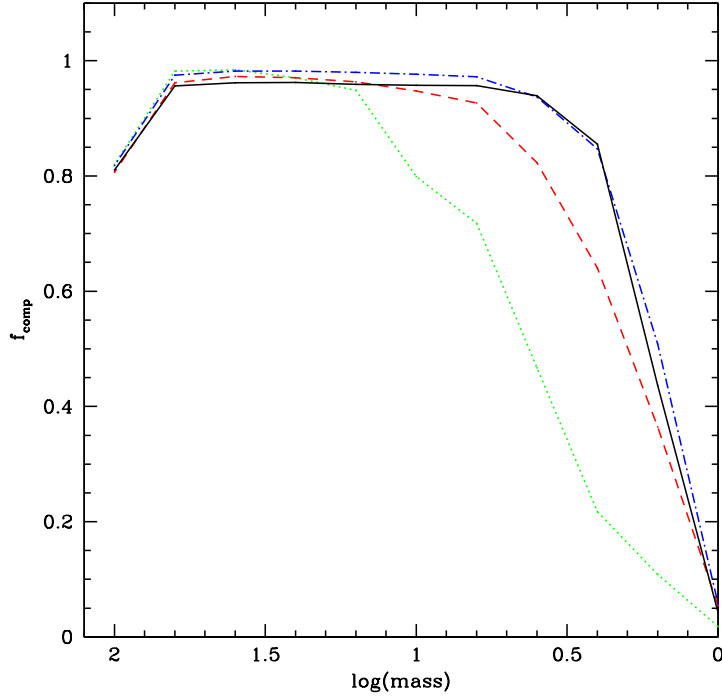


Figure 2. Completeness fraction f_{comp} as a function of the stellar mass (in solar masses) of the stars on the PC chip. The uncertainty of the logarithmic stellar mass is ± 0.2 . The green dotted line denotes the f_{comp} distribution for a circle with a radius of $r < 5''$ around the center of the HD 97950 cluster. The dashed line shows the completeness fraction for the next larger annulus between $5''$ to $10''$, the dot-dashed line indicates f_{comp} for the annulus between $10''$ to $15''$, and the solid line is for the region outside $r > 15''$. The drop in completeness at the high-mass end is primarily due to saturation. Moreover, crowding effects, occasional closeness to the chip boundaries or the location in the overlap areas between the chips all contribute to the completeness fraction never reaching 1.

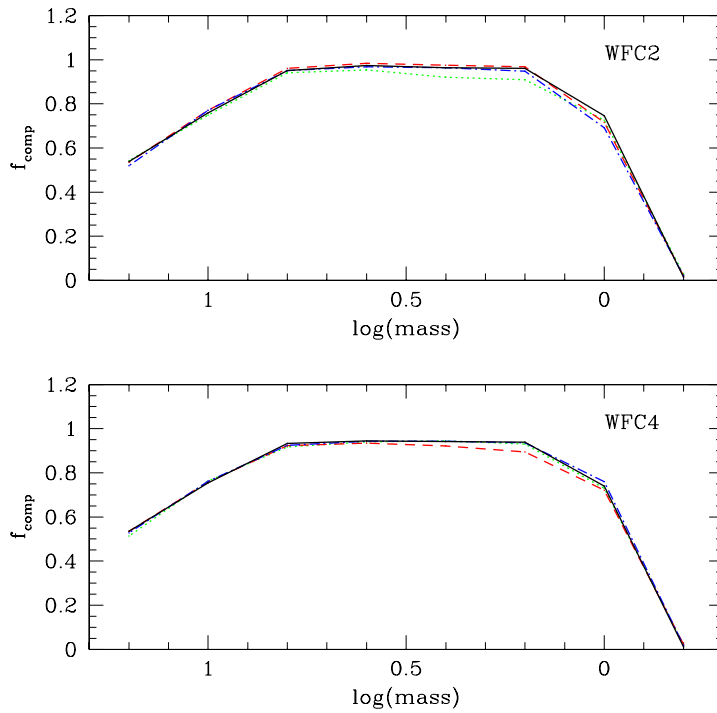


Figure 3. Completeness fraction f_{comp} as a function of magnitude V of the stars on the WFC chips. The green dotted line denotes the f_{comp} distribution for an annulus between $15''$ to $25''$ around the center of the HD 97950 cluster. The dashed line shows the completeness fraction for the next larger annulus between $25''$ to $35''$, the dot-dashed line indicates f_{comp} for the annulus between $35''$ to $45''$, and the solid line is for the region $45'' < r < 60''$.

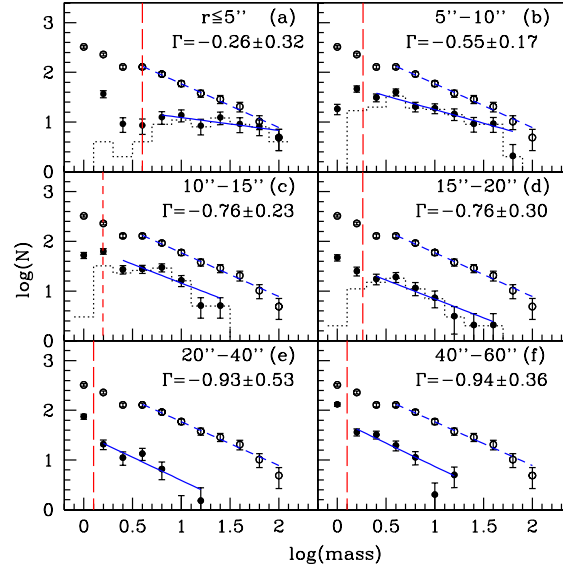


Figure 4. Radial mass function of all cluster member stars on the PC and possible members on the WFC chips. Panels (a) to (f) show mass functions in a sequence of increasing annuli. The dotted histogram is the observed mass function for annuli within $20''$. The filled black dots indicate the mass function corrected for incompleteness and for foreground contamination (panels a–f). The vertical dashed red line indicates a completeness limit of 50%. The blue solid lines show an error-weighted linear least-squares fit of the mass function of each annulus (black filled dots). The short-dashed blue lines are weighted linear least-squares fits to the total mass function (open circles) within $r \leq 60''$. The resulting slope of the total mass function is $\Gamma = -0.88 \pm 0.15$. The slope of the mass function in each annulus is indicated in each panel.

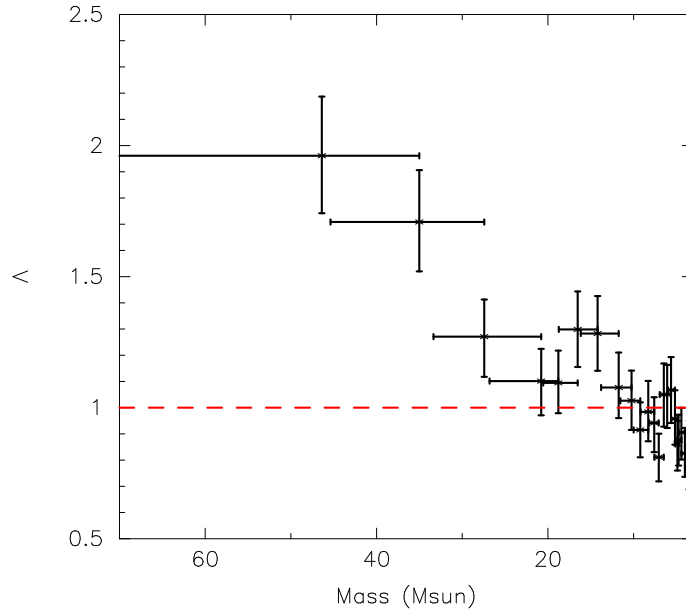


Figure 5. The evolution of Λ along stellar mass. Λ is the ratio of the MST length of 20 random stars over 20 massive stars moving in a declining order of mass and in steps of 10 stars. The vertical bar is 1σ error of Λ . The dashed line indicates a Λ of unity, meaning no mass segregation.

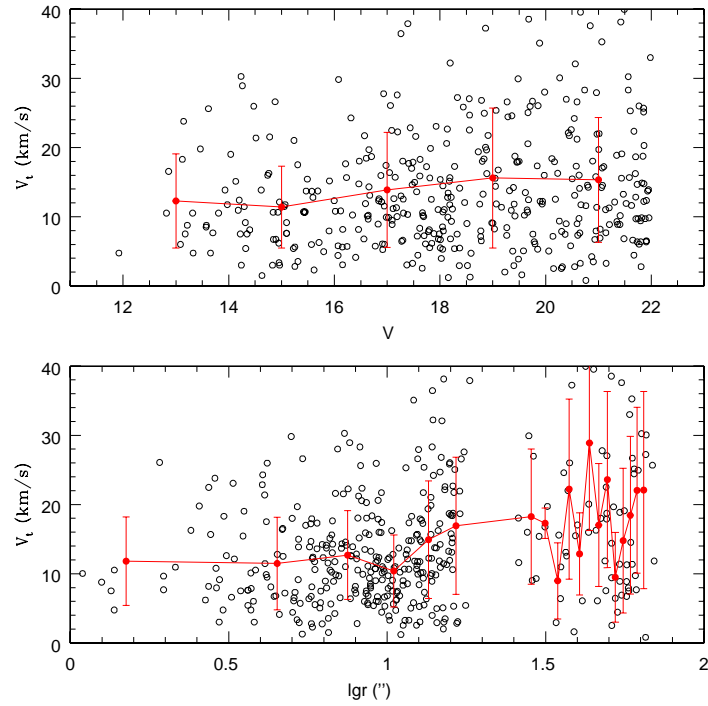


Figure 6. Dependence of the tangential velocity on the V magnitude and the cluster-centric distance. Only stars with a completeness of more than 50% are shown in the plot. The filled dots show the mean velocity in each magnitude bin (binsize = 2 mag; upper panel) and in each annulus (annulus width = $3''$; lower panel). The vertical bar shows the corresponding velocity dispersion.